

Development of Fast Front-End Electronics for the Muon Trigger Detector in the PSI muEDM Experiment

Tianqi Hu, Guan Ming Wong, Sanz Becerra Diego Alejandro, Chavdar Dutsov, Siew Yan Hoh, Kim Siang Khaw, Philipp Schmidt-Wellenburg, Yuzhi Shang, and Yusuke Takeuchi

Abstract—This paper outlines the design and development of a fast front-end electronic readout board for the muon trigger detector in the muEDM experiment at the Paul Scherrer Institute. The trigger detector, which consists of a gate and aperture detector, is strategically located at the end of the superconducting injection channel to generate trigger signals for a magnetic kicker, which activates upon the injection of muons into the central region of the storage solenoid. Within the magnetic field of the solenoid, the system configuration is optimized to meet stringent performance specifications, including minimal signal propagation delays, high detection efficiency, non-magnetic properties, and consistent operational stability under varying experimental conditions. Additionally, the design incorporates robust methods for rejecting positron contamination in the muon beamline. The results presented include performance evaluations from both bench testing and actual beam tests, highlighting the effectiveness and reliability of the electronic design.

Index Terms—Muon electric dipole moment, Radiation detectors, Readout electronics, Signal processing, Trigger circuits

I. INTRODUCTION

THE muEDM collaboration [1], [2] at the Paul Scherrer Institute (PSI) aims to achieve a sensitivity of 6×10^{-23} e·cm in the search for the muon electric dipole moment (EDM) using the “Frozen-Spin” technique [3]. This represents an improvement of four orders of magnitude over the current best limit of 1.8×10^{-19} e·cm set by the Muon $g-2$ Collaboration at Brookhaven National Laboratory [4]. Since the Standard Model prediction of the muon EDM is around 10^{-38} e·cm [5]–[7], any detected signal would clearly indicate physics beyond the Standard Model. Given that the EDM violates time-reversal (T) symmetry, it also violates Charge-Parity (CP) symmetry, assuming CPT symmetry holds. Consequently, the EDM is sensitive to new sources of CP-violation, potentially offering insights into the matter-antimatter asymmetry in the Universe [8].

This work is supported by the National Natural Science Foundation of China under Grant No. 120504102, China Scholarship Council No. 202206230093, and the Horizon EU program EURO-LABS. (Corresponding author: Kim Siang Khaw.)

Tianqi Hu, Guan Ming Wong, Kim Siang Khaw, Siew Yan Hoh, Yuzhi Shang, and Yusuke Takeuchi are with the Tsung-Dao Lee Institute and School of Physics and Astronomy, Shanghai Jiao Tong University, 201210 Shanghai, China (e-mail: hutianqi@sjtu.edu.cn, wong.gm@sjtu.edu.cn, kimsiang84@sjtu.edu.cn, hohsiewyan@sjtu.edu.cn, yz.shang@sjtu.edu.cn, y.takeuchi@sjtu.edu.cn).

Sanz Becerra Diego Alejandro, Chavdar Dutsov, and Philipp Schmidt-Wellenburg are with the Paul Scherrer Institut, Forschungsstrasse 111, 5232 Villigen PSI, Switzerland (e-mail: diego.sanz-becerra@psi.ch, chavdar.dutsov@psi.ch, philipp.schmidt-wellenburg@psi.ch).

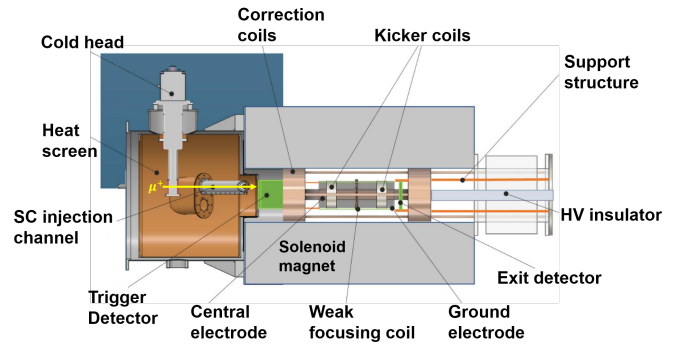


Fig. 1: Conceptual design of Phase I of the PSI muEDM experiment.

The muEDM experiment is divided into Phase-I and Phase-II, where Phase-I is a precursor experiment to demonstrate the frozen-spin technique. Phase-I’s physics goal is to achieve a sensitivity of 3×10^{-21} e·cm. The concept design of the Phase-I experimental setup is illustrated in Fig. 1. A polarized surface muon with a momentum of 28 MeV/c is introduced into a solenoid featuring a 3T magnetic field through a superconducting injection channel [9], where it spirals into the central storage region. This injection method, known as Three-Dimensional Spiral Beam Injection, was proposed by the J-PARC Muon $g-2$ /EDM Experiment [10]. Upon exiting this channel, a muon trigger detector detects the injected muon and sends a trigger signal to the kick coils—two circular coils carrying counter-propagating currents in an anti-Helmholtz configuration [11]. The kick coils generate a pulsed magnetic field that counteracts the muon’s longitudinal momentum, directing the muon into a stable storage orbit within a weakly focusing field created by the weak focusing coil. The activation of the kick coils is carefully synchronized with the muon’s transit through the weakly focusing field. Ultimately, the stored muon will decay into a positron, and the decay process depends on the muon’s spin orientation at the time of its decay. The measurement of the electric dipole moment (EDM) signal will conclude by evaluating the asymmetry in the rates of upward and downward positrons exceeding a specified energy threshold, which varies over time.

The muon trigger detector represents a pivotal element of the experiment, composed of two distinct detectors: the gate detector and a perpendicular aperture detector. Both detectors

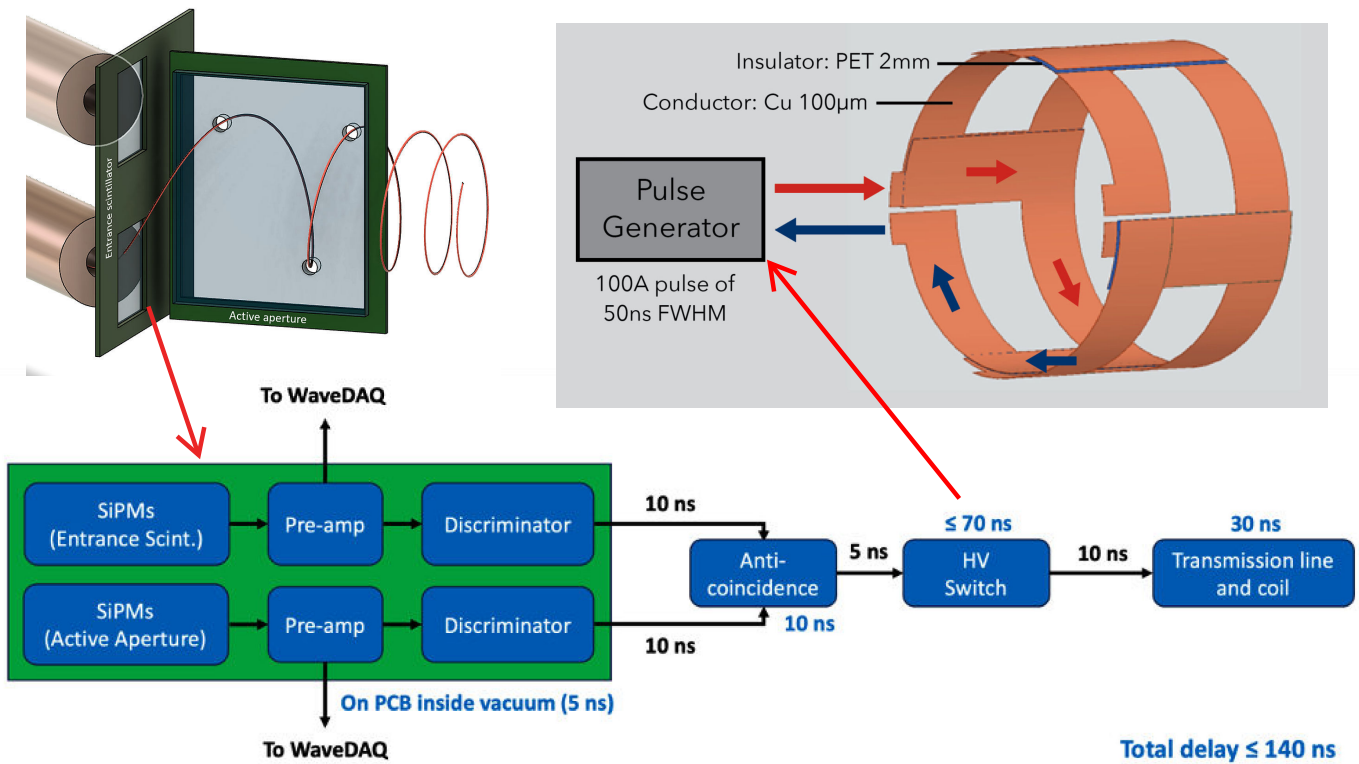


Fig. 2: A schematic layout of the electronic circuit responsible for delivering the current pulse to the kick coils is presented. The structure of the muon trigger detector is illustrated in the upper left corner, whereas the arrangement of the kick coils is depicted in the upper right corner.

are precisely aligned with the nominal reference trajectory of the muons. The gate detector is responsible for identifying the injected muons and generating a trigger signal to activate the switch for the kicker coils. Conversely, the aperture detector inhibits the generation of trigger signals if the muons deviate outside the acceptance criteria established by the solenoid, thus creating an anticoincidence system. This configuration effectively selects muons within the solenoid's acceptance and initiates the brief magnetic pulse required to deflect the muon into its designated storage orbit, thereby reducing the kicker power supply pulse rate from approximately 30 kHz to 1 kHz, which alleviates operational burdens demands.

Furthermore, the detector is optimized to minimize multiple scattering of the detected muons, thereby preserving the quality of the beam as the muons traverse the gate detector. To ensure prompt deflection, it is imperative that the pulsed magnetic field is activated within a latency range of 120 ns to 150 ns, necessitating a rigorous reduction of system-wide delays, particularly within the muon trigger detector and the high-voltage switch of the pulse generator. Additionally, situated within the 3-T solenoidal magnetic field, the front-end readout electronics of the muon trigger detector must

endure high magnetic fields while minimizing any potential interference with the field itself.

This requirement necessitates a robust, non-magnetic design to ensure both precision in timing and stability under experimental conditions. In 2022, a proof-of-concept prototype was developed utilizing plastic scintillators, which are read out by silicon photomultipliers under no-field conditions [12], [13]. Utilizing this prototype, we demonstrated that the selected technology meets the demands of the muEDM experiment. Subsequently, we advanced to the development of an upgraded detector capable of functioning under the actual experimental conditions for Phase I.

This paper examines the research and development efforts behind the electronics of the muon trigger detector, focusing on its design, testing, and performance evaluation. The results demonstrate the detector's successful operation and highlight its capacity to meet the stringent requirements of the muEDM experiment.

II. THE REQUIREMENTS FOR THE MUON TRIGGER DETECTOR

The design of the muon trigger detector is illustrated in Fig. 2. It comprises two identical muon trigger windows and two 0.1 mm for both clockwise (CW) and counter-clockwise (CCW) beam injections. By combining data from both injection directions, one can significantly diminish systematic effects induced by the longitudinal electric field [14]. The aperture detector consists of a scintillator with a thickness of 5 mm, featuring multiple apertures. Muons that fall within the acceptance of the solenoid will traverse these apertures without interacting with the aperture scintillator.

The electronic chain, as shown in Fig. 2, outlines the various contributors to the total pulse latency, which must be carefully controlled to ensure precise timing. The gate and aperture detectors are designed to transmit signals from Silicon Photomultipliers (SiPM) to the WaveDAQ (WaveDream Board) for recording [15], while also generating trigger signals through a discriminator, resulting in an overall latency of approximately 5 ns. These trigger signals are transmitted via coaxial cables and feedthroughs to a coincidence logic unit, introducing an additional delay of 10 ns. The coincidence logic unit processes the input signals and produces a trigger signal to activate the high-voltage (HV) switch for the kick coils, all within 10 ns. A critical aspect of the electronic chain is the internal delay of the HV switch; addressing this delay presents a significant challenge. However, without modifying the overall signal delay, the internal delay specifications for the HV switch can be eased by reducing contributions from all preceding latency sources within the electronic chain, thereby ensuring optimal system performance. Upon activation of the HV switch, the current pulse is transmitted through the vacuum feedthrough, which adds an additional 10 ns, before being conveyed by transmission lines to the center of the solenoid. This timing is meticulously calibrated to ensure that the pulse aligns precisely with the arrival of the muon in storage region.

The electronics of the muon trigger detector must meet stringent performance criteria to ensure successful operation of the experiment. These criteria include minimal latency in signal generation and transmission, compatibility with high-vacuum conditions, and reliable functionality in a high-magnetic-field environment. The electronics' capability to fulfill these specifications is crucial for effectively implementing the muon storage mechanism and achieving broader experimental objectives. The following aspects are particularly important in the design and operation of the electronics:

- The anti-coincidence circuit will be integrated into the muon trigger detector electronics to ensure integrity and reduce the delay contributed by the coaxial cables between these two modules.
- The CW and CCW readout systems share a common circuit to minimize the number of channels.
- The external power supply provides only ± 2.5 V and +3.3 V, while the SiPM operating voltage is achieved through a step-up DC-DC converter.
- The time propagation should be below 15 ns from the detector to the anti-coincidence signal output.

- A splitter circuit is necessary to split the SiPM signals for recording purposes for offline analysis and online discrimination.
- The coincidence efficiency exceeds 95%. Coincidence efficiency refers to the muon hitting both the gate and aperture detectors, represented by the ratio of Zero output from the coincidence module.
- The anti-coincidence efficiency also exceeds 95%. Anti-coincidence efficiency refers to the muon hitting only the gate detector, indicated by the ratio of Non-Zero output from the coincidence module.
- All trigger signals involved are implemented using Low Voltage Transistor-Transistor Logic (LVTTTL) logic levels.

III. DESIGN OF THE ELECTRONICS FOR THE MUON TRIGGER DETECTOR

The schematic diagrams of the electronics for the muon trigger detector, illustrated in Fig. 4, comprise four components: the step-up DC-DC converter, Gate electronics, Aperture electronics, and Anti-coincidence electronics. The Gate and Aperture electronic circuits are similar, with the main difference being that the Gate electronics connect to one SiPM, while the Aperture electronics connect to six SiPMs in parallel with a single output. The Gate Detector employs four SiPMs for CW/CCW readout, resulting in a total of four Gate electronics channels due to the shared electrical channels for CW/CCW readout. In contrast, the Aperture detector requires only one Aperture electronics channel.

A. Step-up DC/DC Converter

A step-up DC/DC converter was utilized to power the SiPMs, as illustrated in Fig. 4(c). The chip used in the circuit is the Analog **LT1615**. The driving voltage is +3.3 V. The output voltage variation over time is displayed in Fig. 3, demonstrating consistent stability in the output voltage. The average output voltage is approximately 32.68 V, with a resolution of $\sigma = 3$ mV. The fluctuation range is 13 mV, which leads to a variation in the SiPM gain being $\sim 0.04\%$.

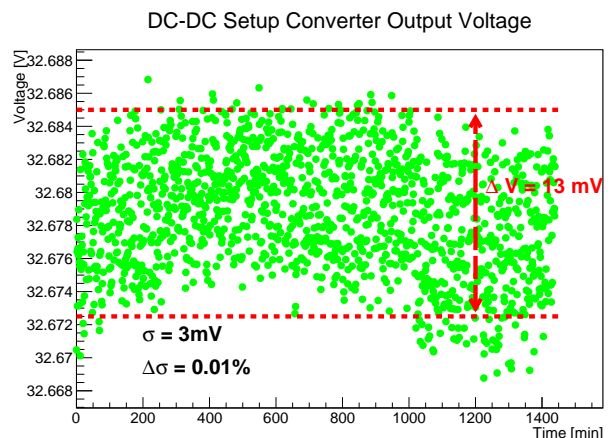


Fig. 3: Output voltage variation of the step-up DC-DC converter.

B. Pre-amplifier Module and Splitter Module

The amplifier chip used in the circuit is the Texas Instruments **LMH6629MF/NOPB**, which has a bandwidth of 900 MHz and a slew rate of 1600 V/ns. The expected gain is calculated as $\frac{620}{10} + 1 = 63$ for the gate and $\frac{200}{10} + 1 = 21$ for the aperture. A 10 nF coupling capacitor is used as the filter.

A splitter circuit consisting of three 16 Ω resistors, placed after the amplifier, is used to divide the amplified signal into two paths. One path directs the signal to the DAQ system for recording, while the other is sent to the discriminator. The splitter distributes the signal, with each path carrying a signal amplified 15.75 times compared to the original SiPM signal, after considering the impedance.

C. Discriminator Module

The discriminator module consists of two main components: the discriminator chip **TLV3801DSGT** and the Low Voltage Differential Signal (LVDS) receiver chip **DS90LV012ATMF/NOPB**. To achieve the shortest propagation delay, the **TLV3801DSGT** LVDS comparator is employed instead of the traditional Transistor-Transistor Logic/Low-Voltage Transistor-Transistor Logic (TTL/LVTTL) discriminator chips; it receives the SiPM signal and generates the LVDS signal. The **DS90LV012ATMF/NOPB** functions as a converter that translates the LVDS signal into the LVTTL signal. A 50 Ω resistor is connected in parallel to the input pin of the **TLV3801DSGT** for impedance matching.

D. Coincidence Module

As illustrated in Fig. 4(d), the coincidence circuit comprises four integrated circuit chips. The LVTTL signals from the SiPMs in the gate detector are routed into the AND logic chip, specifically the **SN74AUC2G08DCUR** from Texas Instruments. The **SN74AUC2G08DCUR** includes two AND gates, each with two inputs. Consequently, the four SiPMs in the gate detector generate two sets of trigger signals, with each pair of SiPMs producing one signal. Similarly, the LVTTL signal from the aperture detector is sent to a NAND logic chip, specifically the **SN74AUC1G00DCKR** from Texas Instruments.

The outputs from these three logic chips are fed into an AND logic chip, the **SN74LVC1G11DCKR** from Texas Instruments. This chip includes one AND gate and three input pins that execute the anti-coincidence operation. This setup enables the coincidence readout of the four SiPMs at the gate detector, effectively determining whether a trigger signal for the HV switch is generated, while the signal from the aperture has the authority to block the generation of this signal.

IV. THE PROTOTYPE BOARDS OF THE ELECTRONICS

The prototype boards for the readout electronics have been produced according to the schematic diagrams presented in Fig. 5 for the gate and aperture electronics boards. The gate board has two windows to accommodate muon injections from Clockwise (CW) and Counter-Clockwise (CCW) directions.

Each window features an ultra-thin EJ-200 scintillator slice measuring $20 \times 20 \times 0.1$, mm³, housed within a $25 \times 25 \times 5$, mm³ acrylic light guide. The light guide is fabricated in our laboratory using Computer Numerical Control (CNC) drilling and grinding techniques to improve photon collection. The four Silicon Photomultipliers (SiPMs) are attached to the center of each side of the light guide with BC-603 optical grease, ensuring efficient detection of the collected photons.

Additionally, two switches have been integrated into the SiPM power supply and signal readout circuits on the gate PCB, allowing for the seamless activation and deactivation of the corresponding SiPMs in both CW and CCW modes. This configuration enables the CW and CCW SiPMs to share a set of readout channels, effectively reducing the total number of electronic channels from eight to four. Moreover, at the gate detector, the signal line lengths for the CW and CCW SiPMs have been adjusted to match, ensuring that all signals reach the coincidence circuit simultaneously, unaffected by variations in path lengths. The SiPM signal from the splitter output in the gate PCB was observed, as shown in Fig. 6; the signal exhibits a strong linear response, with 4 mV corresponding to a single photoelectron. The stable operation of the SiPM readout circuit has been confirmed.

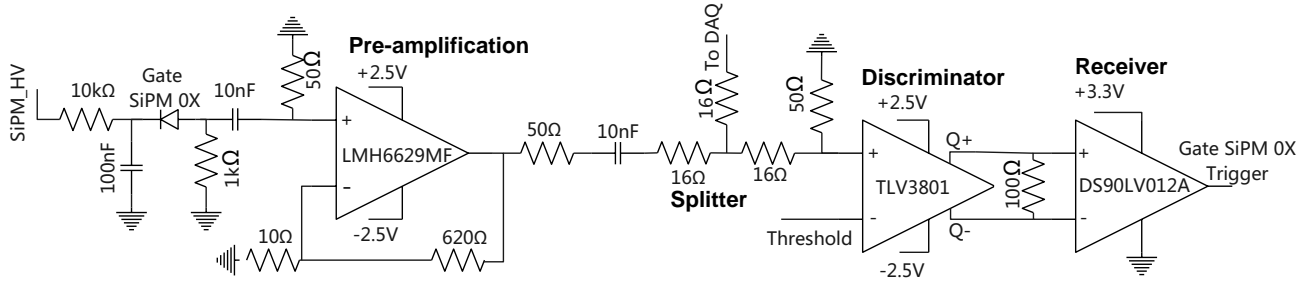
The size and shape of the aperture electronics board are designed according to the dimensions of the scintillator ($130 \times 135 \times 5$, mm³), with the six SiPMs positioned where the maximum photon count occurs at the edge, based on simulation results. The six SiPMs are connected in parallel to a single output, mainly to minimize the number of channels required, as their primary function is to provide trigger signals. This configuration results in a six-fold reduction in internal resistance and a six-fold increase in internal capacitance. Consequently, the signal amplitude decreases, and the rise time increases, with the amplitude of a single photoelectron corresponding to 0.67 mV. However, this arrangement is sufficient for the intended purpose of generating trigger signals. Communication with the gate detector is established through ribbon cables, while the anti-coincidence circuit is embedded in the gate detector's circuit board to manage both coincidence and anticoincidence operations.

V. BEAM TEST AT PSI $\pi E1$ AND RESULTS

From October 28 to November 5, 2024, the muon trigger detector prototype, along with its fast electronics readout circuit, underwent a week-long beam test at the PSI $\pi E1$ beamline, where tests were conducted on positrons and muons. Figure 7 illustrates the setup of the muon trigger detector, highlighting how the exit detector records the particles' tracks after they pass through it. To prevent optical crosstalk between the gate scintillator and the aperture scintillator, the aperture scintillator was coated with 0.1 mm thick aluminum foil. The detectors are located at the bore of the solenoid, which generates a uniform magnetic field of 780 mT.

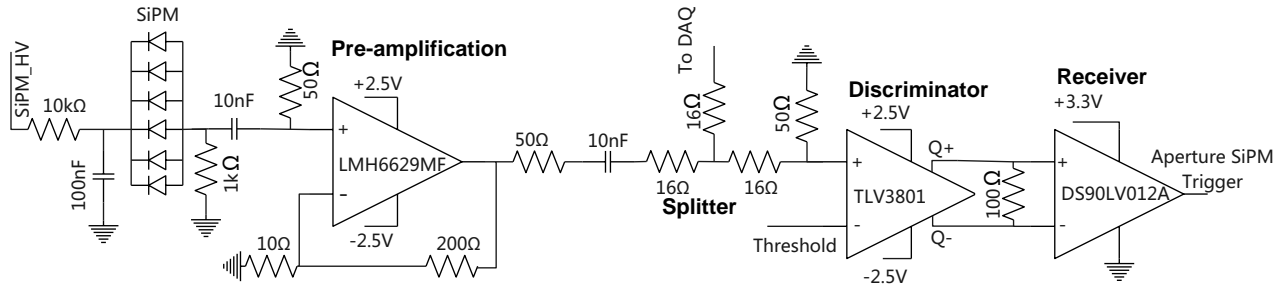
The positron and muon were emitted from the beamline, first passing through a 20 cm air gap, then traveling through the injection tube, which consists of 800 mm tubes with an inner diameter of 15 mm that define the initial collimation, before

Gate SiPM Electronics Readout



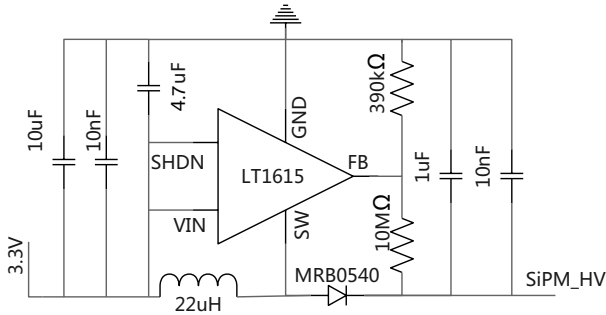
(a) Gate detector readout circuit

Aperture SiPM Electronics Readout



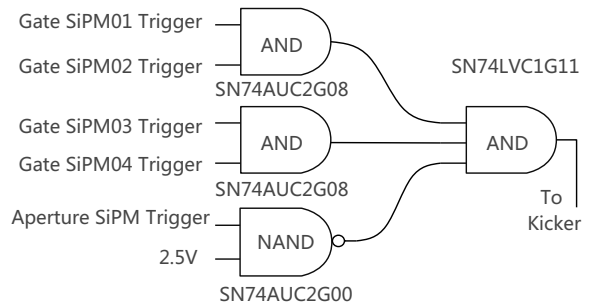
(b) Aperture detector readout circuit

Step-up DC-DC Converter



(c) Electronics for the step-up DC-DC converter

Anti-Coincidence Circuit



(d) Anti-Coincidence Circuit

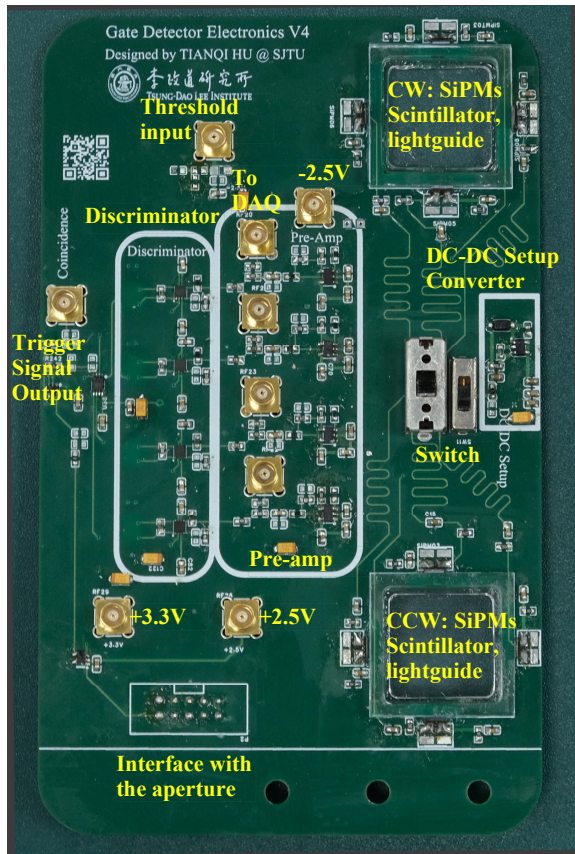
Fig. 4: Simplified schematic of the SiPM readout

reaching the muon trigger detector. Upon arrival at the muon trigger detector, the positrons had a momentum of 7 MeV/c, while the muons had a momentum of 22.5 MeV/c. Particles within the acceptance range of the muon trigger detector pass through the holes in the aperture scintillator and continue to the exit detector. In contrast, particles outside this range are stopped and absorbed by the aperture scintillator.

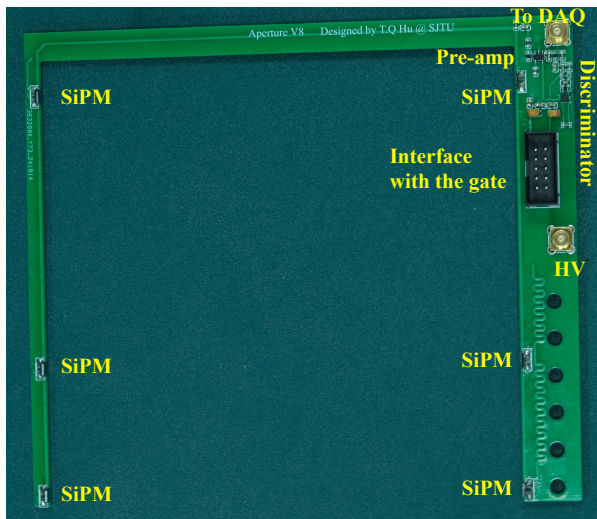
Utilizing the WaveDAQ system for data acquisition [15], the standard waveforms collected for coincidence (when both the gate and aperture detectors are activated) and anticoincidence (when exclusively the gate detectors are activated) are depicted in Fig. 8.

The propagation delay is defined as the time interval during

which all SiPM signals exceed the threshold (10 mV for e^+ , 15 mV for μ^+) to the half-height of the rising edge of the LVTTTL trigger signal output. The results of the propagation delay for both CW and CCW muons, as well as positrons, are presented in Fig. 9, with an average of 5.92(0.48) ns. More importantly, the electronics remained stable under the magnetic field environment and during long-term operation, as indicated by the datasets of the CW/CCW μ^+/e^+ at different time points, showing no significant discrepancies in the propagation delay measurements. The error bar for the μ^+ is smaller than that for the e^+ for two main reasons: first, the statistics for the μ^+ are ten times greater than those for positrons; second, the DAQ settings and beam tuning for the

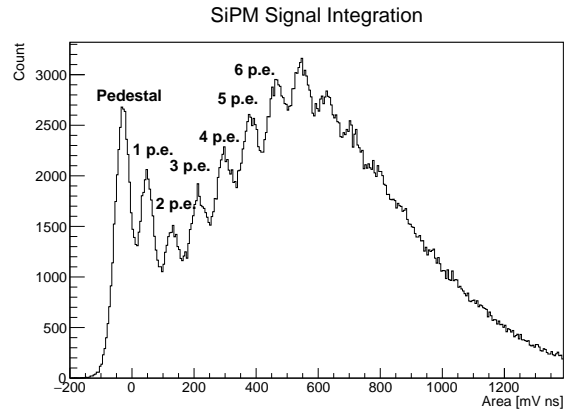


(a) A completed PCB board for the gate detector. All the electronic components are shown, including the step-up DC-DC converter, discriminator, and trigger signal output.

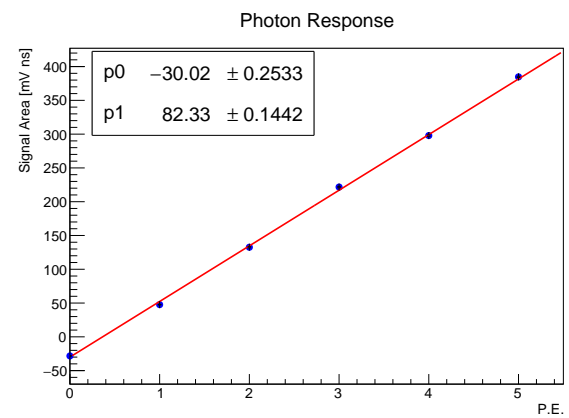


(b) A completed PCB board for the aperture detector. All electronic components are displayed, including the interface with the gate, discriminator, and pre-amplifier.

Fig. 5: Completed PCB boards for the muon trigger detector.



(a) Photon peaks



(b) Photon Response Linearity

Fig. 6: Tested the linearity of the SiPM signals after the splitter output using an Am-241 radioactive source at the gate scintillator slice

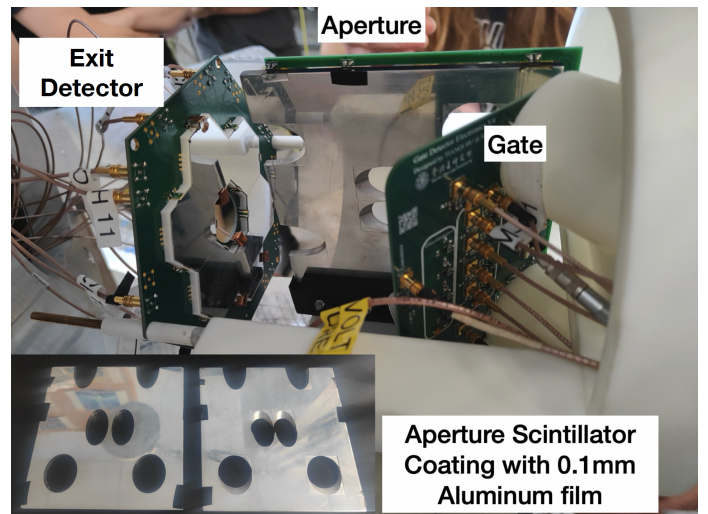
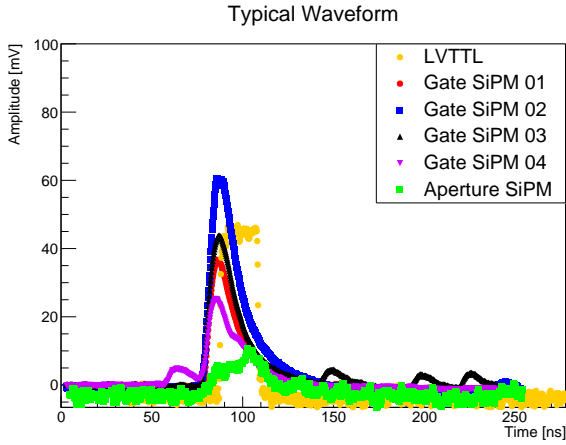
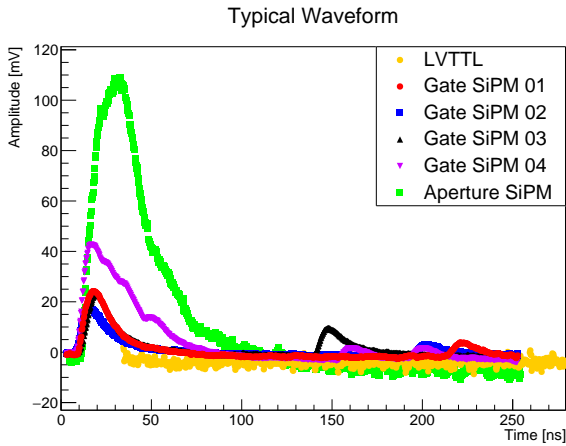


Fig. 7: Muon trigger detector prototype for the Beam Test 2024 at the PSI $\pi E1$ beamline.



(a) Waveform for Anti-Coincidence Trigger. The e^+ hits only the gate detector and results in the trigger signal output.



(b) Waveform for Coincidence Trigger. The e^+ hits both the gate and aperture detector, in which the aperture signal prevents the production of the trigger signal.

Fig. 8: Typical waveform recorded by WDB for the muon trigger detector, with positron injected. Note that the LVTTL trigger signal cable is equipped with an attenuator providing 20 dB attenuation.

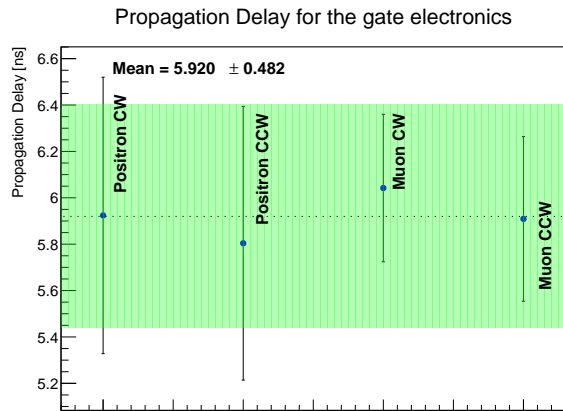


Fig. 9: Propagation delay results for the Beam test 2024.

μ^+ were optimized compared to those for e^+ .

The anti-coincidence efficiency of the detector is defined as the effectiveness of the electronics in outputting LVTTL trigger signals under anticoincidence conditions. When a particle strikes the gate detector and successfully passes through the holes of the aperture detector, a trigger signal should be generated, as illustrated in Fig. 8(a). Figure 10 shows the distribution of the anti-coincidence efficiency for the datasets. The anti-coincidence efficiency for μ^+ exceeds 99%, while for e^+ it exceeds 98%. The reasons for the discrepancy are twofold:

- 1) The hysteresis of the discriminator requires the signal amplitude to exceed a threshold value of approximately 2 mV to activate the discriminator. For instance, with a 10 mV threshold, the discriminator activates only when the signal exceeds about 12 mV. This results in a 1-2% ratio of anticoincidence cases where, even though the signal amplitude surpasses the discriminator threshold, it does not overcome the hysteresis, thus preventing the trigger signal from being output.
- 2) The energy deposition within the gate detector is greater for the positively charged muons (μ^+) than for the positrons (e^+), with average energy depositions recorded as $\bar{E}_{\mu^+} = 0.272$ MeV and $\bar{E}_{e^+} = 0.017$ MeV, respectively. As a result, the signals generated by the silicon photomultipliers (SiPM) from the μ^+ exhibit a larger amplitude, facilitating their ability to exceed the threshold and surpass the hysteresis of the discriminator.

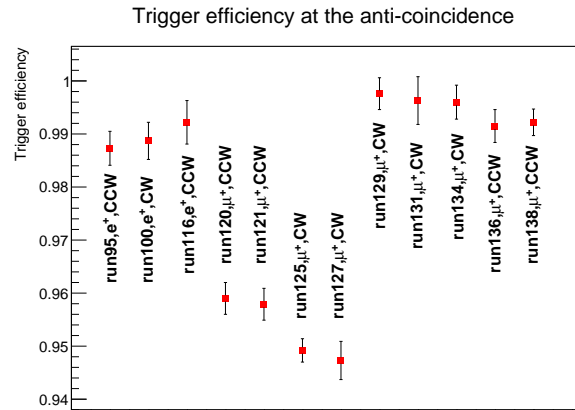


Fig. 10: Anti-coincidence efficiency for the μ^+ and e^+ datasets under various conditions. It should be noted that for datasets run120, run121, run125, and run127, the separator of the beamline was found to be turned off, as most of the μ^+ events in these datasets are contaminated by the e^+ .

The efficiency of coincidence is defined as the probability that the aperture detector prevents the output of LVTTL trigger signals under conditions of coincidence. When a particle strikes both the gate and the aperture detector, the signal generated by the aperture detector should inhibit the production of the trigger signal, as depicted in Fig. 8(b). In the context of coincidence events, 97.38% (5.05%) did not result in the output of the LVTTL trigger signal, whereas 2.62%

(0.83%) of coincidence events did generate the LVTTL trigger signal. Although these unexpected LVTTL trigger signals may activate the pulsed magnetic field, no muons are emitted, as they remain confined within the aperture scintillator. Consequently, the data acquisition system records the events as empty. Assuming that 95% of the muons successfully enter the storage area, the proportion of empty events would amount to less than 0.1% of the total events. Should the success rate decrease to 90%, this proportion would increase to less than 0.3%, and at a success rate of 80%, it would be less than 0.6%. These empty events may be excluded through offline analysis or alternative methods.

The failure of coincidence primarily arises from the substantial capacitance resulting from the parallel configuration of six SiPMs in the aperture detector, which leads to an extended rise time of the SiPM signal. As a consequence, approximately 2.62(0.83)% of the coincidence events possess time windows for the aperture trigger signal that do not completely coincide with those of the gate trigger signal, resulting in the generation of a narrow LVTTL trigger width.

The electronics properties are detailed in Tab. I, meeting the requirements of the PSI muEDM experiment. The next steps will focus on further optimizations, such as refining the wiring of the aperture SiPMs, adjusting the connections and cable lengths between the gate and aperture, adding a temperature feedback module, and more. These enhancements will establish the foundation for the upcoming beam test in 2025.

TABLE I: Properties of the muon trigger detector prototype and PSI muEDM requirements.

| | Electronics Board | muEDM requirements |
|-----------------------------|-------------------|--------------------|
| Anti-Coincidence efficiency | 99.5% | $\geq 95\%$ |
| Coincidence efficiency | 97.4% | $\geq 95\%$ |
| Propagation delay [ns] | 5.9 ± 0.5 | ≤ 15 |
| Trigger Signal Voltage [V] | 2.5 | > 1.7 |
| Trigger Signal Width [ns] | 20.0 ± 6.0 | > 3 |

VI. CONCLUSION

In this work, we presented the development and performance evaluation of the fast front-end electronics for the muon trigger detector in the PSI muEDM experiment. The system was designed to meet stringent requirements, including minimal signal propagation delays, high detection efficiency, and stable operation under high-magnetic-field conditions. To achieve these objectives, we implemented a custom-designed PCB layout with non-magnetic components, optimized readout circuits, and an anti-coincidence trigger logic to efficiently identify storable muons while rejecting non-storable events.

The beam test conducted at the PSI π E1 beamline validated the performance of the trigger detector and its electronics. The results demonstrated:

- High anti-coincidence efficiency of 99.5% for muons, exceeding the required threshold of 95%.
- Coincidence efficiency of 97.4%, ensuring accurate muon identification.

- Low propagation delay of 5.9 ± 0.5 ns, well within the experimental requirement of ≤ 15 ns.
- Stable operation in the 3-T solenoidal magnetic field, confirming the robustness of the design for future experimental phases.

During extended beamline operations, the system maintained its timing precision and reliability, indicating its suitability for long-term data acquisition in the muEDM experiment. The integration of optimized trigger electronics and low-latency signal processing effectively reduced background contamination and improved the selection of muons for the frozen-spin technique.

Moving forward, we will focus on further refinements in wiring optimizations, reducing capacitance effects in the aperture detector, and integrating temperature feedback mechanisms to enhance long-term stability. These improvements will prepare the detector for Phase I of the PSI muEDM experiment, ensuring high-precision measurements in the search for a muon electric dipole moment.

REFERENCES

- [1] A. Adelman et al. A compact frozen-spin trap for the search for the electric dipole moment of the muon. 1 2025.
- [2] A. Adelman et al. Search for a muon EDM using the frozen-spin technique. 2 2021.
- [3] F. J. M. Farley, K. Jungmann, J. P. Miller, W. M. Morse, Y. F. Orlov, B. L. Roberts, Y. K. Semertzidis, A. Silenko, and E. J. Stephenson. A New method of measuring electric dipole moments in storage rings. *Phys. Rev. Lett.*, 93:052001, 2004.
- [4] G. W. Bennett et al. An Improved Limit on the Muon Electric Dipole Moment. *Phys. Rev. D*, 80:052008, 2009.
- [5] Maxim Pospelov and Adam Ritz. CKM benchmarks for electron electric dipole moment experiments. *Phys. Rev. D*, 89(5):056006, 2014.
- [6] Diptimoy Ghosh and Ryosuke Sato. Lepton Electric Dipole Moment and Strong CP Violation. *Phys. Lett. B*, 777:335–339, 2018.
- [7] Yasuhiro Yamaguchi and Nodoka Yamanaka. Large long-distance contributions to the electric dipole moments of charged leptons in the standard model. *Phys. Rev. Lett.*, 125:241802, 2020.
- [8] A. D. Sakharov. Violation of CP Invariance, C asymmetry, and baryon asymmetry of the universe. *Pisma Zh. Eksp. Teor. Fiz.*, 5:32–35, 1967.
- [9] Anastasia Doinaki et al. Superconducting shield for the injection channel of the muEDM experiment at PSI. *JINST*, 18(10):C10011, 2023.
- [10] Kodai Oda et al. Developments of a Pulse Kicker System for the Three-Dimensional Spiral Beam Injection of the J-PARC Muon g-2/EDM Experiment. *JACoW*, IPAC2021:726–729, 2021.
- [11] Timothy Hume, Ritwika Chakraborty, Anastasia Doinaki, Chavdar Dutsov, Massimo Giovannozzi, Katia Michielsen, Ljiljana Morvaj, Angela Papa, Philipp Schmidt-Wellenburg, and David Stäger. Implementation of the frozen-spin technique for the search for a muon electric dipole moment. *JINST*, 19(01):P01021, 2024.
- [12] Guan Ming Wong, Jun Kai Ng, Tianqi Hu, Meng Lyu, and Kim Siang Khaw. Research and development of a muon entrance trigger for the muEDM experiment at PSI. *Nucl. Part. Phys. Proc.*, 346:58–62, 2024.
- [13] Tianqi Hu, Jun Kai Ng, Guan Ming Wong, Cheng Chen, Kim Siang Khaw, Meng Lyu, Angela Papa, Philipp Schmidt-Wellenburg, David Staeger, and Bastiano Vitali. Beam test performance of a prototype muon trigger detector for the PSI muEDM experiment. 12 2024.
- [14] G. Cavoto et al. Anomalous spin precession systematic effects in the search for a muon EDM using the frozen-spin technique. *Eur. Phys. J. C*, 84(3):262, 2024.
- [15] Marco Francesconi et al. The WaveDAQ integrated Trigger and Data Acquisition System for the MEG II experiment. *Nucl. Instrum. Meth. A*, 1045:167542, 2023.